BULLETIN OF THE POLISH ACADEMY OF SCIENCES
TECHNICAL SCIENCES, Vol. 68, No. 4, 2020
DOI: 10.24425/bpasts.2020.134184

Fatigue life prediction for acid-resistant steel plate under operating loads

T. TOMASZEWSKI[1]*, P. STRZELECKI[1], M. WACHOWSKI[2], and M. STOPEL[1]

[1] University of Science and Technology, Faculty of Mechanical Engineering, 7 Prof. S. Kaliskiego Street, 85-796 Bydgoszcz, Poland
[2] Military University of Technology, Faculty of Mechanical Engineering, 2 Gen. Urbanowicza Street, 00-908 Warsaw, Poland

Abstract. The paper evaluates the causes related to the fatigue damage in a conveyor slide plate, exposed to high-frequency cyclic loads. The plate was made of 1.4301 acid-resistant steel. The fractography showed that the plate failure was caused by fatigue crack. A nonlinear analysis of plate deformation was conducted using the finite element method (FEA) in LS-Dyna software. The maximum normal stresses in the plate fracture were used in further analysis. A "fatigue limit" calculated initially using a FITNET procedure was above the maximum stress calculated using FEA. It indicates that the structural features of the plate were selected correctly. The experimental test results for 1.4301 acid-resistant steel were described using a probabilistic Weibull distribution model. Reliability was determined for the obtained S-N curve at 50% and 5% failure probability allowing for the selected coefficients (cycle asymmetry, roughness, variable load) and the history of cyclic loading. Cumulative damage was determined using the Palmgren-Miner hypothesis. The estimated fatigue life was similar to the actual value determined in the operating conditions for the S-N curve at 5% failure probability. For engineering calculations, the S-N curve at max. 5% failure probability is recommended.

Key words: reliability, macro-fractography, finite element analysis, S-N curve, acid-resistant steel.

1. Introduction

Structural and mechanical components under operating loads are susceptible to fatigue damage. The cyclic nature of loading may cause the initiation and propagation of cracks, an example of theses experimental tests can be found in [1]. If the structural component area under heavy load is subject to cyclic loading, faulty design may result in decohesion and machine failure. It may lead to additional costs, and in the worst-case scenarios, for instance, to a railway accident [2]. The damage is often caused by manufacturing, material or design defects, incorrect fatigue limit calculations, overload, or other operational issues. Fatigue damage is caused due to operating loads [3, 4], further leading to loss of structural functionality.

Due to the effect of multiple factors on the propagation of fatigue failure, it is crucial to define the actual operation conditions at the design stage, allowing for the factors affecting the durability of the designed component. Standards, guidelines, directives, and regulations based on the general deterministic models, and correction coefficients are usually applied at the design stage. The fatigue properties of any material represented as an S-N curve for unnotched material specimens are corrected based on the experimentally determined coefficients (e.g. surface finishing coefficient, notch, size, shape and cycle asymmetry, defects) and the S-N curve is determined for the structural component [5–10]. Despite numerous fatigue tests conducted since the end of the 19th century, the cracking of structural components under variable load still occurs [11–13]. Attempts are made to explain the failure causes for new components tested under controlled operating conditions, e.g. a crankshaft for ship engine [14]. If the structural component failure may cause accidents, the fatigue tests of complete machines, e.g. planes [15] or bogie frames [16] are required.

The study analyses the operating conditions of a steel slide plate used in a belt conveyor. The plate was subject to variable load resulting in the propagation of fatigue crack and premature failure. The study analysed the structure for the correct design of the component based on the actual operating conditions. A fatigue limit was estimated based on material data and numerical calculations. The cracks were analysed under bending loads.

2. Specimen

The analysis was conducted for a slide plate used in a drop packer. The plate was subject to high-frequency operating loads. The operating conditions caused premature crack propagation and failure. The plate was made of 1.4301 cold-rolled 3 mm thick acid-resistant steel. The plates were prepared using laser cutting technology. The plate edges were bent on a bending brake at an internal bending radius of 3 mm. Figure 1 shows the geometry of the tested plate. The plate was used as a slide component in the belt conveyor. Figure 2 show the operation diagram. The analysed unit is used for packaging products (bottles (2)) into a cardboard box (3). The top conveyor feeds and buffers the product. A specific number of products is dropped (1) from the top conveyor. To reduce the product impact on the slide plate (4), the conveyor with the cardboard is lifted.

*e-mail: tomaszewski@utp.edu.pl

Manuscript submitted 2020-03-17, revised 2020-04-17, initially accepted for publication 2020-05-06, published in August 2020

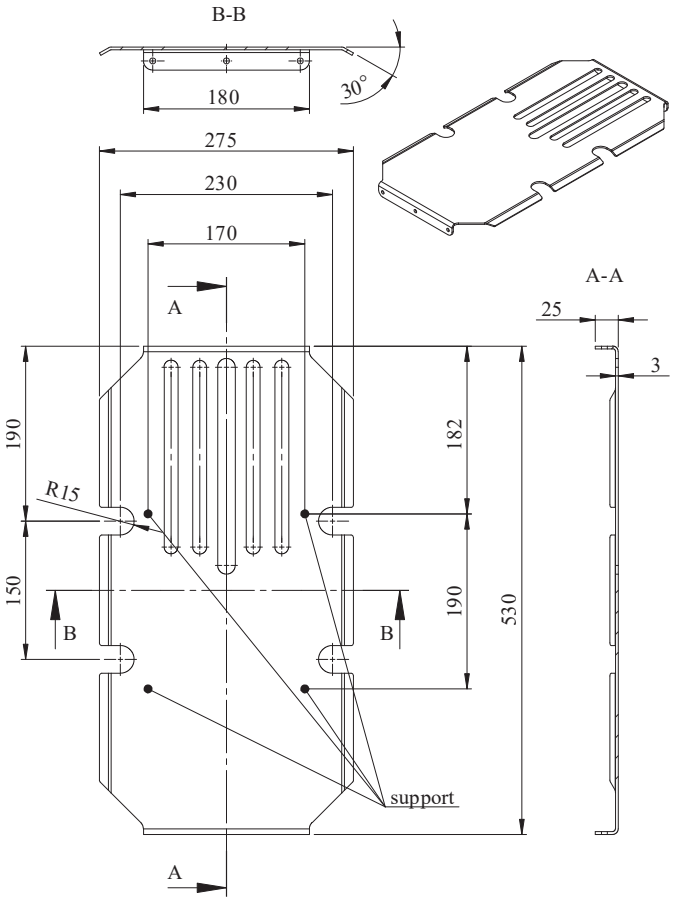

Fig. 1. Plate geometry and dimensions in mm

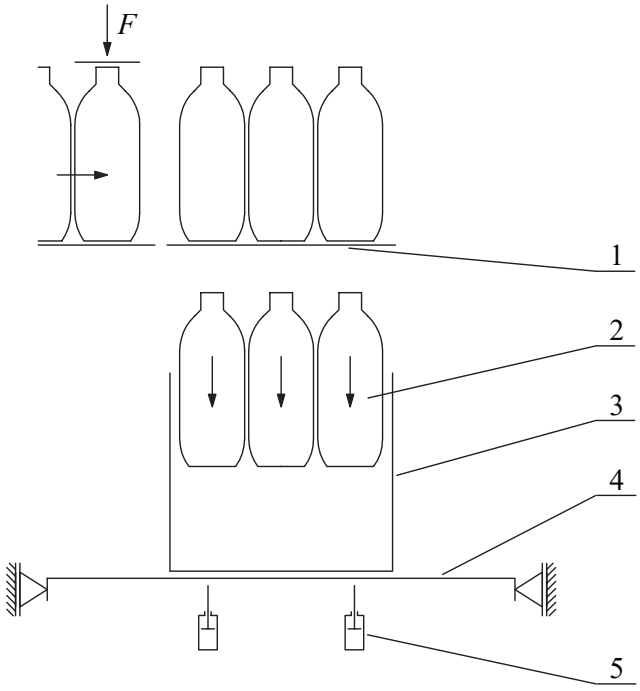

Fig. 2. Plate load and support diagram in the drop packer: 1 – top conveyor, 2 – bottle, 3 – cardboard box, 4 – analysed slide plate, 5 – damping element

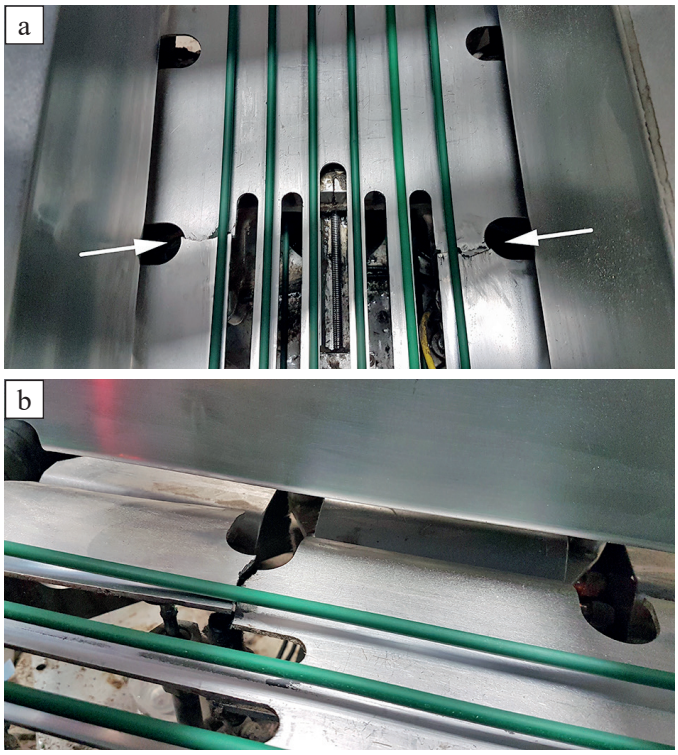

Fig. 3. Plate fracture: a) general view, b) detailed view of the crack

A dampening unit (5) is installed under the slide plate to ensure a sufficient deceleration path for the product.

Figure 3 shows cracks in the smallest cross-section of the plate. The plate failed after approx. 8700 hours of operation. The fatigue life was estimated at approx. $4.5 \cdot 10^6$ cycles. The plate was subject to variable maximum stress amplitude resulting from conveying products of different weights.

To estimate the reliability under variable amplitude cyclic stress, a complex load history can be converted into constant amplitude cyclic stresses using the cumulative fatigue assessment. The reliability was calculated based on the fatigue life distribution under variable stress amplitude. Block maximum loads corresponding to the transport of bottle packs with different weights (9 kg, 6 kg, 4.5 kg, 3 kg, 2.4 kg) were used in the analysis. Fig. 4 shows the operating load history.

In all load cases, the bottles contacted the plate after traveling a distance of 0.4 m. The dampening unit decelerated the product at a maximum distance of 0.015 m. The product falling rate was 2.8 m/s. The kinetic energy before impact equals the gravitational potential energy corresponding to the falling height of the load. The average force of impact F was determined analytically based on the work-energy principle according to the equation:

$$F = \frac{mgh}{d}, \tag{1}$$

where m is the mass of the object, g is the gravitational acceleration, h is the drop height, d is the distance travelled after impact. A maximum impact force for a 9 kg load was 2352 N.

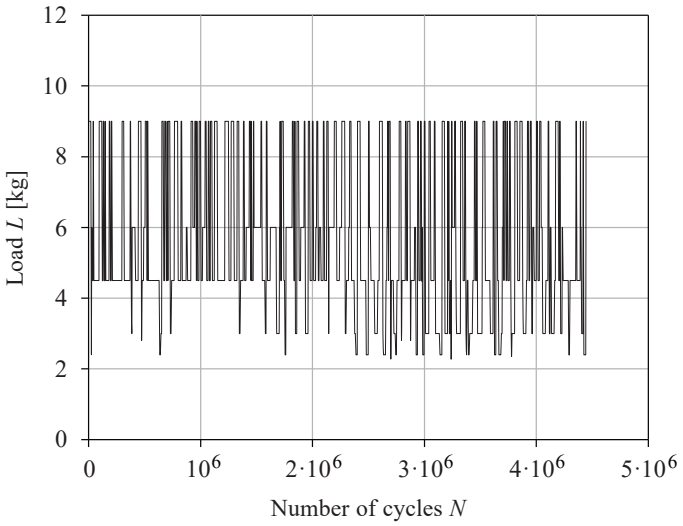

Fig. 4. Operating load history of plate

3. Experimental test methods and results

3.1. Macro-fractography. The observations of fracture surfaces were conducted to evaluate the mechanism of crack propagation in the plate. The cracks were analysed using a JEOL JSM-6610 electron scanning microscope (JEOL, Tokyo, Japan) in a secondary electron mode (SE). The observations were performed at 15 kV acceleration voltage. SEM images in Figs. 5 and 6 show the fracture area of the specimen subjected to fatigue.

The front of the crack in the specimens was observed in the corner, corresponding to the higher stress concentration in this section. The crack propagation stopped on the opposite side of the specimen (left).

The fractographic analysis showed that the crack was irregular throughout the specimen. At the crack initiation stage, striation-like marking and fissure-type striations were observed. Fig. 6a shows the termination of crack propagation at the grain boundaries. The stages of stable crack growth and unstable cracking with dislocation slip were observed. Numerous microcracks at the junction of slip bands and secondary cracks were also observed. Fig. 6b shows the fatigue striations.

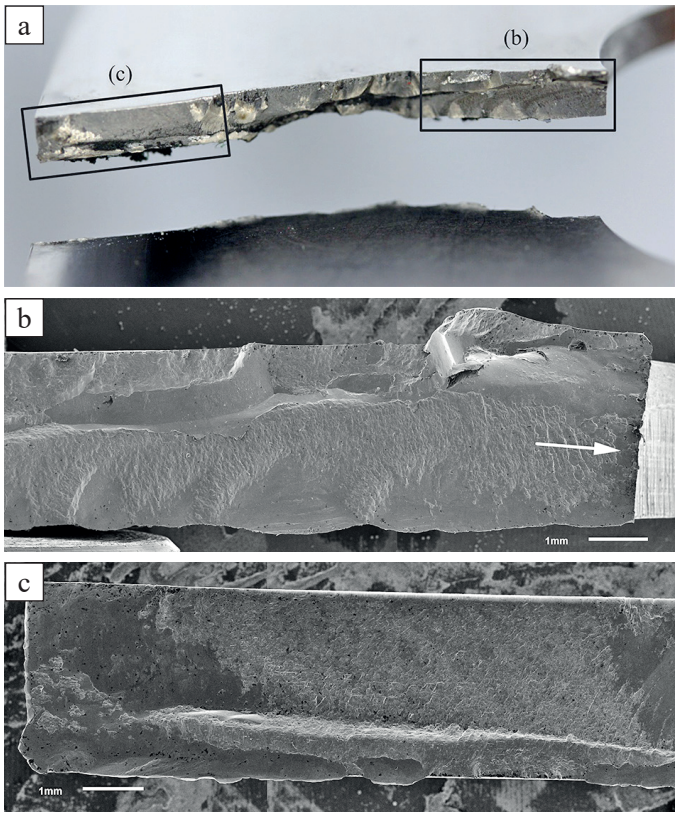

Fig. 5. Fracture areas of the plate: a) overall fracture surface, b) right side, c) left side; the arrow indicates maximum normal stress in the cross-section of the plate

3.2. Material and chemical composition. The specimen was made of austenitic 1.4301 acid-resistant steel. Due to a rel-

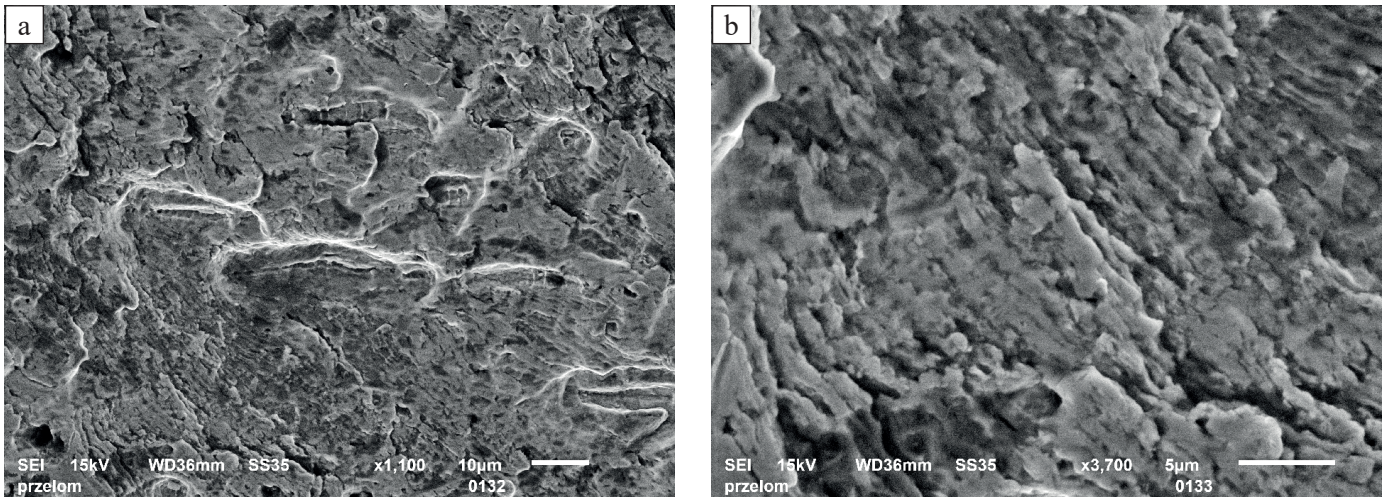

Fig. 6. SEM fractography of 1.4301 acid-resistant steel: a) propagation region, b) striation marks

atively good ratio of mechanical properties, machinability, availability and price, this material is commonly used in the food industry machines. The mechanical properties of this material are susceptible to various factors, e.g. its mechanical and fatigue properties depend on its size. The difference in fatigue life was noticeable and verified experimentally for the minispecimens [17].

The 1.4301 steel features significantly higher content of alloying elements compared to other commonly used steels. In the statistical size effect approach, it may translate into a higher probability of occurrence of the potential fatigue crack initiation points. Thickness and size may significantly affect the fatigue limit. The analysed steel was delivered as a cold-rolled 4 mm thick sheet. Table 1 shows the chemical analysis results.

Table 1
Chemical composition of the 1.4301 steel

C, %	Si, %	M, %	P, %	S, %	C, %	Ni, %	N, %
0.02	0.41	1.54	0.028	0.001	18.1	8.1	0.051

The carbon content in the tested specimen was very low (0.02%). The corrosion resistance is affected by chromium and nickel content, 18.1% and 8.1%, respectively.

The static tensile test was conducted on an Instron 8874 testing machine in accordance with PN-EN ISO 6892-1:2016 [18]. The tests were conducted using a force gauge with ±25 kN measuring range and 2620 Instron axial extensometer with a base unit of 25 mm and the elongation range of ±5 mm. Figure 7 shows the geometry of the unnotched specimens used in the monotonic tensile test.

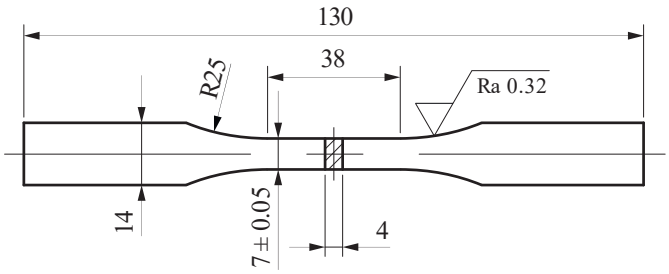

Fig. 7. Geometry of the unnotched specimen for monotonic tensile test made of 1.4301 acid-resistant steel, dimensions in mm

Nonlinear stress-strain behavior described by the Ramberg-Osgood equation:

$$\varepsilon = \frac{\sigma}{E} + 0.002\left(\frac{\sigma}{R_{0.2}}\right)^{n}, \tag{2}$$

where ε is the strain, σ is the stress, $R_{0.2}$ is the 0.2% proof stress as the equivalent yield stress, E is the initial elastic modulus and n is the strain hardening exponent. The value of the initial elastic modulus E is obtained by a linear regression least-squares estimate of the slope in the proportional elastic region.

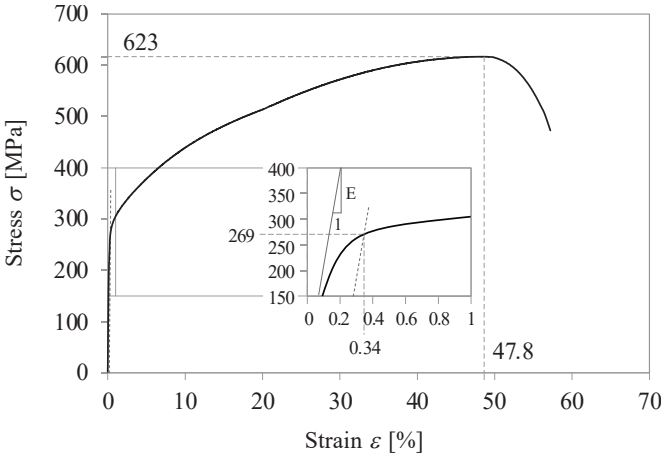

Fig. 8. Stress-strain curve for 1.4301 steel

The average measured values and standard deviation for the three specimens are presented in Table 2 (modulus of elasticity E, tensile strength R_m, yield strength $R_{0.2}$, reduction of area Z, longitudinal elongation A, strain hardening exponent n). The tested material showed high ductility. Figure 8 shows the quasi-static characteristic (ε–σ curve) for 1.4301 steel.

Table 2
Mechanical properties of the 1.4301 steel

Parameter	E, MPa	$R_{0.2}$, MPa	R_m, MPa	Z, %	A, %	n
Value	200 195	269	623	77.1	69.5	7.1
Std dev	2645	3.1	4.9	0.5	1.3	1.0

Figure 9 shows the microstructure of the tested material. Visible austenite grains are approx. 40 µm. The microstructure of the material was evaluated using OLYMPUS LEXT OLS4100 Confocal Laser Scanning Microscope (Olympus, Tokyo, Japan).

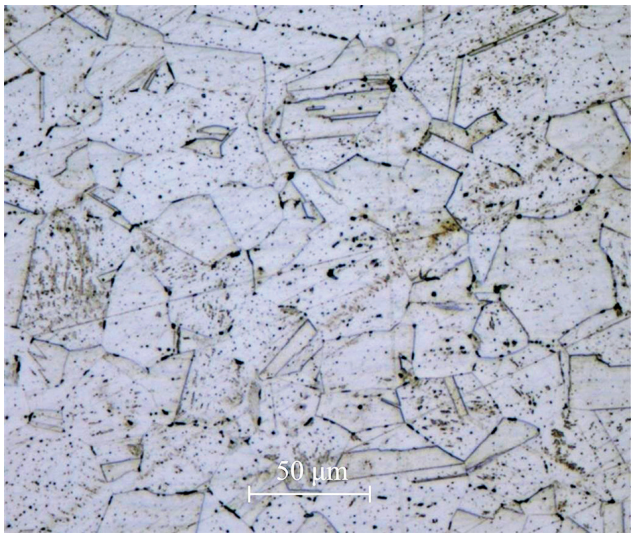

Fig. 9. Microstructure of the analysed 1.4301 acid-resistant steel

Prior to the structural analysis, the specimen was subjected to metallographic preparation involving grinding on SiC abrasive papers, 240 to 2400 grade and polishing with 3 μm and 1 μm diamond suspensions.

3.3. Numerical method. A finite element analysis in LS-Dyna software was conducted to determine the stress distribution within the plate. FEA is commonly used to analyze the stress distribution in an operating structure [19]. LS-Dyna is a dedicated environment used for the analysis of dynamic phenomena featuring a high non-linearity [20] using an explicit integration method. The use of the explicit integration method which does not require transposing the stiffness matrix to solve the system of equations reduces the calculation time, which in this case depends on the number of independent variables. The explicit integration method was used due to the high non-linearity of the analysed phenomena and contact between the model elements.

The numerical model was developed in LS-PrePost. The geometry was divided into 77 866 finite elements. In total mesh consisted of 79 105 nodes. Two types of elements were used, structural shells and discrete elements.

Structural 4-nodes shells (*SHELL) with Belytschko-Lin-Tsay formulation (*ELFORM type 16) were used to model the plate and the bottles. They were fully integrated elements with 2×2 in-plane integration points with three integration points through-thickness. The element stresses were calculated in those integration points and then extrapolated to nodes. The results were taken from outermost integration points then averaged at nodes for smooth representation (Fig. 11).

Discrete 2-nodes elements (*DISCRETE) were used to model damping units. For those elements, material cards *SPRING_ELASTIC, and *DAMPER_VISCOUS were used accordingly for a spring and a damper. For those elements displacement and forces were calculated at nodes.

The average element size was 2 mm in length with aspect ratio no larger than 2.5 for the most distorted elements due to mesh transitions and there were no more than 14 (0.018%) elements with poor Jacobian (greater than 0.6). The relative ratio of the element size to the overall geometry was $2\cdot10^{-5}$. Furthermore, the element size was chosen in reference to the radiuses of notches occurring in the model accordingly to the literature [21] and did not adversely affect the results. For so prepared mesh only simple check for mesh discretization was conducted which proved that further refinement will not influence results much and achieved computation time was acceptable.

The model was fixed by removing all degrees of freedom from the nodes at both ends of the damping unit (see Fig. 10). The damping element head can move along the y-axis only. The load is a bottle pack (9 kg, 6 kg, 4.5 kg, 3 kg, 2.4 kg) falling from a height of 0.4 m by gravity. The values used correspond to the actual conditions shown in Section 2.

The contact conditions without friction were established between the system elements, i.e. slide plate and bottles and slide plate and damping element head. *CONTACT_SURFACE_TO_SURFACE card was used. The analysis duration was 0.1 s with a $7.1\cdot10^{-7}$ step. The plate model used a mathematical material model allowing for the plasticity (density 7.86 g/cm^3, Young's modulus $2.1\cdot10^5$ MPa, Poisson ratio 0.3, yield point 269 MPa).

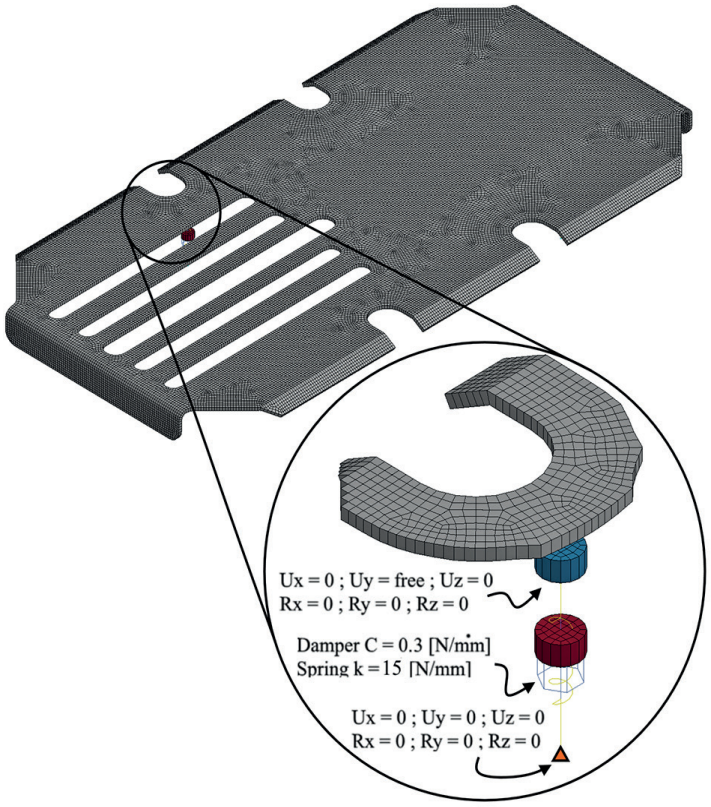

Fig. 10. Damping and boundary conditions

The stress distribution maps were analysed for several product impact stages. Figure 11 shows the highest stress for 9 kg load.

The normal stress distribution maps correspond to the fatigue failure location. The analyses showed stress concentration in the smallest cross-section of the plate. Table 3 shows

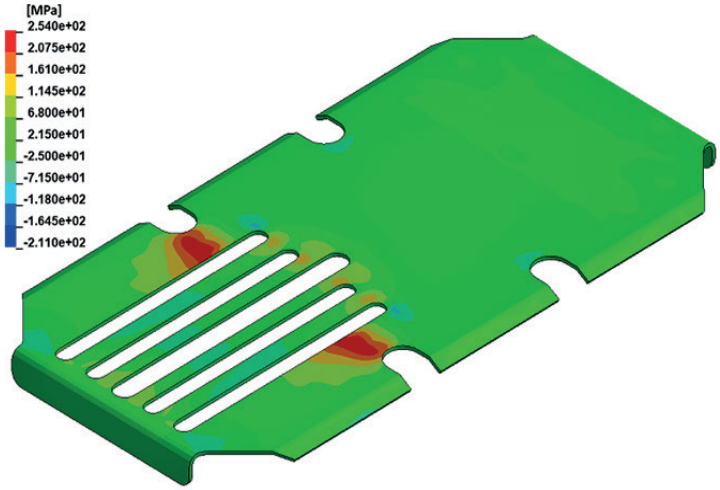

Fig. 11. Normal stress distribution map in the plate for 9 kg load

Table 3
Numerical calculation values

Load, L (kg)	Force, F (N)	Max. deflection, f (mm)	Max. normal stress, S (MPa)
9	2611	15.35	242.7
6	2298	11.05	222.6
4.5	2066	8.53	198.9
3	1721	6.32	168.4
2.4	1520	5.37	152.9

the calculated values for all analysed load cases. The numerical calculations were used to determine the maximum normal stress for each load level. The values were used in further analytical calculations. The damping element stiffness was identical in all cases. Change in the maximum normal stress is non-linear since it depends on the constant damping element stiffness.

Further FEA included evaluation of the modelled damping and stiffness properties. The used values corresponded to the parameters of the damping elements used in the actual machine. A significant reduction in the maximum stress was observed in the area of stress concentration.

3.4. Fatigue analysis. An initial evaluation of the fatigue life was conducted based on one of the commonly used FITNET engineering procedures [5]. The S-N curve for a limited fatigue life is established by determining the fatigue limit for the material σ_W from the following equation:

$$\sigma_W = f_{W,\sigma} \cdot R_m, \tag{3}$$

where $f_{W,\sigma}$ is a fatigue strength factor provided by the procedure depending on the material and R_m is the tensile strength of the material. Coefficients $f_{W,\sigma}$ for the analysed acid-resistant steel are 0.4. Using the tensile strength of the analysed material (623 MPa) in (3) gives 249.2 MPa. To determine the fatigue limit at 10^6 cycles for the structural element σ_{WK} the following equation was used:

$$\sigma_{WK} = \sigma_W \cdot K_d \cdot \eta_\sigma \cdot K_{S,\sigma}, \tag{4}$$

where K_d is the element size coefficient, $K_{S,\sigma}$ is the effect of surface roughness on fatigue limit and η_σ is the notch effect on fatigue life that depends on the stress gradient. K_d is equal to 1 for analysed dimensions of the element. The calculated value of η_σ was 0.957 (the stress gradient equal to 0.195). The last coefficient was the value defining the effect of surface roughness on fatigue limit (K_S) was calculated as 0.88 ($Rz = 1.6$ µm in the plate which fulfils requirements of [22]). Using those values in (4) gives the fatigue limit for the structural element of 187.9 MPa at 10^6 cycles, which is for the asymmetry of $R = -1$. For the cycle asymmetry of $R = 0$ must be corrected. The FITNET procedures prosed using the Walker model for calculated the effect of mean stress by the following formula:

$$M = 10^{-3} a_\psi R_\psi + b_\psi, \tag{5}$$

where a_ψ, b_ψ are material constants and are 0.35 and –0.1, respectively. R_ψ is the ultimate strength (non-dimensional). The fatigue limit for the structural element for the asymmetry of $R = 0$ σ_{AK} is 176.8 MPa. A double value of permissible stress amplitude of 353.6 MPa was used to determine the stress range ΔS. Figure 12 shows the S-N curve determined by the FITNET method.

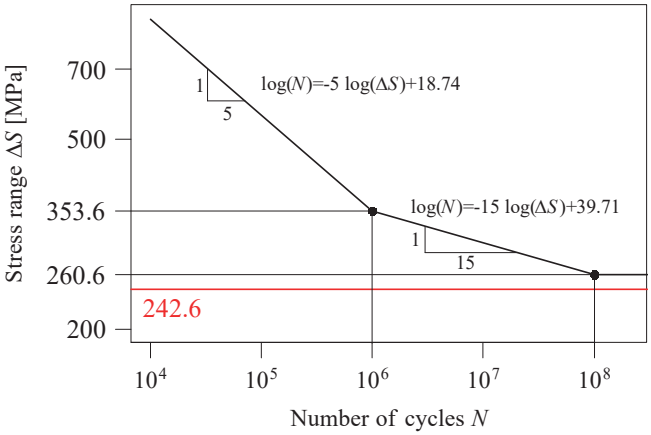

Fig. 12. The S-N curve determined by the FITNET method with marked stress estimated by FEA, the maximum normal stress form FEA for 9 kg – 242.7 MPa

A slope rate of 15 was used for 10^6 to 10^8 cycles, and the slope rate of 5 was used for the fatigue life below 10^6 cycles, which is recommended by the FITNET method. More information about the slope coefficient can be found in [23] and [24]. The maximum stress obtained based on the FEA calculation is marked with a red line. This value is lower than the fatigue limit determined analytically, corresponding to the unlimited fatigue life. It shows that the analysed element should not fail. The authors decided to follow up with the experimental tests.

Further evaluation of the causes of plate failure included analyses based on the experimental test results. Figure 13 shows unnotched specimens made of the same steel as the plate (1.4301 acid-resistant steel).

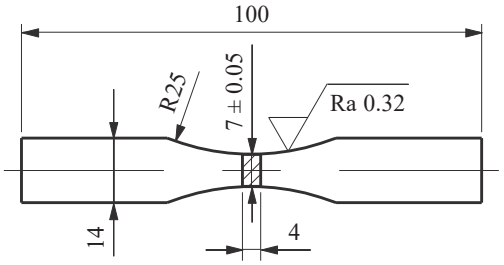

Fig. 13. Geometry of the unnotched specimen for fatigue testing made of 1.4301 acid-resistant steel

The analysis aimed to determine the S-N curve for a load-controlled test. The scope of the tests covered high-cycle fatigue. The end of the test criterion was a micro-fracture of the specimen. The load was applied by the repeating bending with the cycle asymmetry of $R = -1$. The tests were conducted in accordance with standard requirements [25, 26]. The fatigue tests were conducted using Instron 8874 hydraulic testing machine. Figure 14 shows the test results (black circles). 8 specimens were used for the experiment. A set of 7 specimens is recommended in the standard [18]. The tests were conducted for 4 the stress amplitude (400 MPa, 440 MPa, 480 MPa and 480 MPa) and 2 specimens for each stress level.

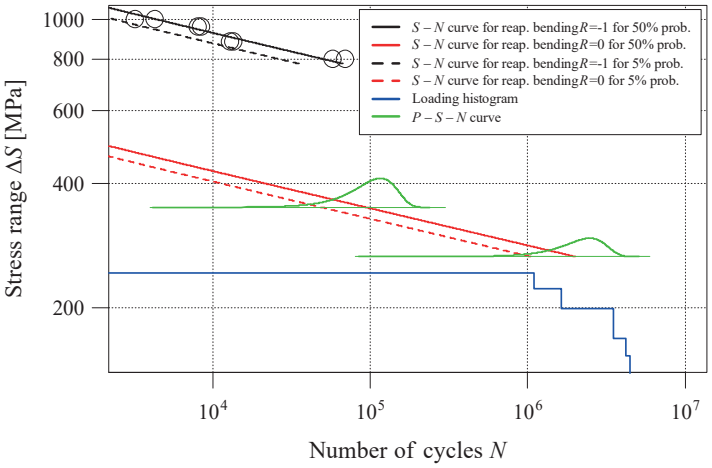

Fig. 14. S-N curve for 1.4301 steel

The experimental points were approximated using a probabilistic model for the selected failure probabilities. This parameter can be represented by a 3-parameter Weibull cumulative distribution function for general stress applied and expressed as follows [27]:

$$F_{-1} = 1 - \exp\left[-\left(\frac{N-\xi}{\theta}\right)^{\alpha}\right], \tag{6}$$

where θ is a scale parameter, α is a shape parameter and ξ is a location parameter. For mean stress equal 0 ($R = -1$):

$$F_0 = 1 - \exp\left[-\left(\frac{N_0-\xi_0}{\theta_0}\right)^{\alpha_0}\right], \tag{7}$$

For other mean stress values:

$$F_0 = 1 - \exp\left[-\left(\frac{N_1-\xi_1}{\theta_1}\right)^{\alpha_1}\right], \tag{8}$$

Assuming that the shape α and the location ξ parameters are common and only differ in the scale parameter θ for two stress distributions:

$$\begin{aligned} &1 - \exp\left[-\left(\frac{N_0-\xi_0}{\theta_0}\right)^{\alpha_0}\right] = \\ &= 1 - \exp\left[-\left(\frac{\sigma_{a0}}{\sigma_{a-1}}\right)^{\alpha_0}\left(\frac{N_1-\xi_0}{\theta_1}\right)^{\alpha_0}\right], \end{aligned} \tag{9}$$

where σ_{a0} is fatigue strength for asymmetry stress $R = 0$ and σ_{a-1} is fatigue strength for asymmetry stress $R = -1$.

Assuming that the Weibull distribution describes the S-N curve, the location parameter $\xi(\sigma_{ai})$ is $10^{m\cdot\log(\sigma_{ai})+d}$ and the scale parameter $\theta(\sigma_{ai})$ is $10^{a\cdot\log(\sigma_{ai})+b}$, where b is a constant term in the S-N curve equation, d is a constant term in the S-N curve equation in the location parameter, a is a slope coefficient in the S-N curve equation and m is a slope coefficient in the S-N curve equation in the location parameter. Finally, the equation for the S-N curve is:

$$F(N) = 1 - \exp\left[-\left(\frac{(N_i)-\xi(\sigma_{ai})}{\theta(\sigma_{ai})}\right)^{\alpha_1}\right], \tag{10}$$

It is assumed that the slope of the S-N curve at different mean stress values is the same (based on the FITNET method) due to small differences in slope for $R = -1$ and $R = 0$ in [28]. The final estimated S-N curve for different asymmetry stresses can be expressed as:

$$\begin{aligned} b_{-1} &= b_0 + \log\left[-\left(\frac{\sigma_{a0}}{\sigma_{a-1}}\right)^{\alpha}\right] \text{ or} \\ b_0 &= b_{-1} - \log\left[-\left(\frac{\sigma_{a0}}{\sigma_{a-1}}\right)^{\alpha}\right]. \end{aligned} \tag{11}$$

Equation (11) was discussed in detail in [29]. The operating load of the plate resulted from free falling bottles, translating into a one-sided load change cycle. The results of the experimental tests for a symmetrical cycle were converted into the one-sided cycle. The effect of mean stress can be calculated using the Walker model by (5).

For the cycle asymmetry of $R = 0$, the (5) is:

$$\left(\frac{\sigma_{a0}}{\sigma_{a-1}}\right)^{\alpha} = \left(1 - \left(\frac{M}{2}\right)\right)^{\alpha}, \tag{12}$$

The fatigue life was reduced by 40% [30] to allow for the laser cutting effect. The maximum load was variable and depended on the configuration and size of the bottles. The S-N curve was offset by a value corresponding to the effect of variable load on fatigue life in accordance with the following equation [31]:

$$\mathrm{SSF} = \log\left[\sum n_i / \sum n_i \cdot \left(S_{a,i}/S_{a,max}\right)^{a}\right], \tag{13}$$

where n_i is the number of cycles at i-th load level, $S_{a,i}$ is the load amplitude at the i-th load level and a is the slop.

Figure 14 shows the S-N curve (red line) determined using (10), shifted by (12) and (13) and the formula of the distribution is as follows:

$$F_0(N) = 1 - \exp\left[-\left(\frac{(N_i) - 10^{-1.05 \cdot \log(\sigma_{ai}) + 4.95}}{10^{-11.1 \cdot \log(\sigma_{ai}) + 33.1}}\right)^4\right], \quad (14)$$

A black line shows the S-N curve determined using (11) for cycle asymmetry $R = -1$ and the formula of the distribution is as follows:

$$F_{-1}(N) = 1 - \exp\left[-\left(\frac{(N_i) - 10^{-1.05 \cdot \log(\sigma_{ai}) + 4.95}}{10^{-11.1 \cdot \log(\sigma_{ai}) + 33.7}}\right)^4\right], \quad (15)$$

It was assumed that the load is applied in $q = 5$ stages (242.7 MPa, 222.6 MPa, 198.6 MPa, 168.4 MPa, 152.9 MPa, in accordance with FEA calculations – Table 3). The number of load cycles for each stage was (1 100 400; 537 600; 1 887 200; 655 200; 263 233 cycles), respectively for each load level. A load histogram is shown as the blue line in Fig. 14.

A Palmgren-Miner linear damage hypothesis was used in the next calculation stage:

$$D = \sum_{i=1}^{q} \frac{n_i}{N_i}, \quad (16)$$

where n_i is the number of cycles for a load stage at i-th load level, N_i is the number of cycles based on the S-N curve for a load stage shown in Fig. 14 (red line).

The cumulative damage was 0.53. The FITNET procedure recommends using permissible value $D = 0.5$. The structural element failed at the cumulative failure above 0.5, which validates the assumption. Since the S-N curve at 50% failure probability should not be used in engineering calculations, additional calculations were conducted using (16) and the S-N curve at 5% failure probability (red dashed line, Fig. 14). A value of $D = 1.02$ was obtained. The value is similar to the limit value of 1 taken in the original version of the Palmgren-Miner hypothesis.

4. Conclusion

In this paper, the fatigue life and reliability of a slide plate were estimated. The following conclusions can be drawn:

- The fractography showed that plate failure was caused by fatigue damage. A striation mark, characteristic of the fatigue crack propagation was observed.
- Each stage of product falling on the plate was verified by the FEA. The maximum stress occurred in the fatigue crack location. The calculated stress values were within 242.7÷152.9. The initial verification using the FITNET procedure showed that the maximum stress values obtained using FEA were lower than the fatigue limits determined using the analytical methods. The correct structural features of the plate were selected.
- Fatigue properties were analysed using the probabilistic model based on the Weibull distribution. The S-N curves at 5% and 50% failure probability where used. The cumulative damage according to the Palmgren-Miner hypothesis was 1.02 and 0.53, respectively. The calculations showed that the plate should fail for the S-N curve at 5% failure probability after a number of cycles corresponding to the actual operating conditions (approx. $4.5 \cdot 10^6$ cycles). For the most commonly used S-N curve at 50% failure probability, the number of cycles was approx. $8.4 \cdot 10^6$.

Further studies should aim to determine the safety factor for fatigue life calculations. Unfortunately, the FITNET procedure does not specify the value that should be used in the calculations. Using the correct safety factor in (4) would show that the slide plate has a limited fatigue life. The 3-parameter Weibull distribution can be used to determine the S-N curve for any failure probability. For engineering calculations, the S-N curve at max. 5% failure probability is recommended. For each designed machine, the value should be selected individually. An example approach was presented in [32].

References

[1] M. Kotyk, D. Boroński, and P. Maćkowiak, "The Influence of Cryogenic Conditions on the Process of AA2519 Aluminum Alloy Cracking," *Materials (Basel).* 13(7) 1555 (2020).

[2] H.A. Richard, M. Fulland, M. Sander, and G. Kullmer, "Fracture in a rubber-sprung railway wheel," *Eng. Fail. Anal.* 12(6), 986–999 (2005).

[3] H.A. Richard, M. Sander, B. Schramm, G. Kullmer, and M. Wirxel, "Fatigue crack growth in real structures," *Int. J. Fatigue* 50, 83–88 (2013).

[4] C.R. Gagg and P.R. Lewis, "In-service fatigue failure of engineered products and structures – Case study review," *Eng. Fail. Anal.* 16(6), 1775–1793 (2009).

[5] M. Kocak, S. Webster, J. Janosch, J., A. Ainsworth, and R. Koers, "FITNET Fitness-for-Service PROCEDURE – FINAL DRAFT MK7," 2006. http://www.fracture.tu.kielce.pl/procedury_2/Section0.pdf

[6] Y.-L. Lee, J. Paw, B. Hathaway, R.B. Hathaway, and M.E. Barkey, *Fatigue Testing and Analysis – Theory and Practice*. Elsevier Butterworth–Heinemann, 2005.

[7] P. Strzelecki and J. Sempruch, "Verification of analytical models of the s-n curve within limited fatigue life," *J. Theor. Appl. Mech.* 54(1), 63 (2016).

[8] M. Wachowski, L. Śnieżek, I. Szachogłuchowicz, R. Kosturek, and T. Płociński, "Microstructure and fatigue life of Cp-Ti/316L bimetallic joints obtained by means of explosive welding," *Bull. Pol. Ac.: Tech.* 66(6), 925–933 (2018).

[9] Y. Ai *et al.*, "Probabilistic modeling of fatigue life distribution and size effect of components with random defects," *Int. J. Fatigue* 126, 165–173 (2019).

[10] D. Liao, S.P. Zhu, J.A.F.O. Correia, A.M.P. De Jesus, and F. Berto, "Recent advances on notch effects in metal fatigue: A review," *Fatigue Fract. Eng. Mater. Struct.* 43(4), 637–659 (2020).

[11] S.K. Bhaumik, R. Rangaraju, M.A. Venkataswamy, T.A. Bhaskaran, and M.A. Parameswara, "Fatigue fracture of crankshaft of an aircraft engine," *Eng. Fail. Anal.* 9(3), 255–263 (2002).

[12] H.A. Richard, M. Sander, M. Fulland, and G. Kullmer, "Development of fatigue crack growth in real structures," *Eng. Fract. Mech.* 75(3–4), 331–340 (2008).

[13] A.A. Shaniavskiy and A.L. Toushentsov, "Mechanisms of fatigue crack initiation and propagation in cast aluminum alloy AL5 of hydropumps NP-89D in aircraft Tu-154M," *Eng. Fail. Anal.* 17(3), 658–663 (2010).

[14] M. Fonte and M. de Freitas, "Marine main engine crankshaft failure analysis: A case study," *Eng. Fail. Anal.* 16(6), 1940–1947 (2009).

[15] N. Iyyer, S. Sarkar, R. Merrill, and N. Phan, "Aircraft life management using crack initiation and crack growth models – P-3C Aircraft experience," *Int. J. Fatigue* 29(9–11), 1584–1607 (2007).

[16] Y. Lu, H. Zheng, J. Zeng, T. Chen, and P. Wu, "Fatigue life reliability evaluation in a high-speed train bogie frame using accelerated life and numerical test," *Reliab. Eng. Syst. Saf.* 188(March), pp. 221–232, 2019.

[17] T. Tomaszewski and P. Strzelecki, "Study of the size effect for non-alloy steels S235JR, S355J2+C and acid-resistant steel 1.4301," in *AIP Conference Proceedings*, 201, p. 020008.

[18] PN-EN ISO 6892–1:2016, "Metallic materials – Tensile testing – Part 1: Method of test at room temperature," 2016.

[19] P. Baranowski and J. Malachowski, "Numerical study of selected military vehicle chassis subjected to blast loading in terms of tire strength improving," *Bull. Pol. Ac.: Tech.* 63(4), 867–878 (2015).

[20] D. Skibicki, Ł. Pejkowski, and M. Stopel, "Finite Element Analysis of Ventilation System Fire Damper Dynamic Time-History," *Polish Marit. Res.* 24(4), 116–123 (2017).

[21] A. Cichanski, "Mesh size dependency on notch radius for FEM analysis of notched round bars under tension," *AIP Conf. Proc.* 1822, 020004, 2017.

[22] ISO-9013, "Thermal cutting — Classification of thermal cuts — Geometrical product specification and quality tolerances," Geneva, 2002.

[23] C.M. Sonsino, "Course of SN-curves especially in the high-cycle fatigue regime with regard to component design and safety," *Int. J. Fatigue* 29, 2246–2258 (2007).

[24] P. Strzelecki, J. Sempruch, and K. Nowicki, "Comparing guidelines concerning construction of the S-N curve within limited fatigue life range," *Polish Marit. Res.* 22(3), 67–74 (2015).

[25] ISO-12107, "Metallic materials – fatigue testing – statistical planning and analysis of data," Geneva, 2012.

[26] PN-H-04326:1796, "Fatigue tests of metals – Bending tests," 1976.

[27] W. Weibull, *A statistical theory of the strength of materials* 151. Stockholm, 1939.

[28] G. Szala and B. Ligaj, *Two-parameter fatigue characteristics of construction steels and their experimental verification* (in Polisch). Bydgoszcz: Uniwersytet Technologiczno-Przyrodniczy im. J.J. Śniadeckich – Instytut Technologii Eksploatacji – PIB, 2011.

[29] T. Tomaszewski, P. Strzelecki, A. Mazurkiewicz, and J. Musiał, "Probabilistic Estimation of Fatigue Strength for Axial and Bending Loading in High-Cycle Fatigue," *Materials (Basel).* 13, 1148 (2020).

[30] D.F. Pessoa, P. Herwig, A. Wetzig, and M. Zimmermann, "Influence of surface condition due to laser beam cutting on the fatigue behavior of metastable austenitic stainless steel AISI 304," *Eng. Fract. Mech.* 185, 227–240 (2017).

[31] P. Heuler and H. Klätschke, "Generation and use of standardised load spectra and load-time histories," *Int. J. Fatigue* 27, 974–990 (2005).

[32] S.P. Zhu, Q. Liu, W. Peng, and X. C. Zhang, "Computational-experimental approaches for fatigue reliability assessment of turbine bladed disks," *Int. J. Mech. Sci.* 142–143, 502–517 (2018).